Interplay of Various Charge Sources in AlGaN/GaN Epi-Stack Governing HEMT Breakdown

Ankit Soni and Mayank Shrivastava, *Senior Member, IEEE*

Abstract— **In this work, we have revealed the interplay of various charge sources (surface, polarization, and buffer) and their relative concentrations across the AlGaN/GaN epi-stack governing the electric field distribution and the breakdown mechanism in high electron mobility transistors (HEMTs). The investigations are carried out for Schottky, metal-insulator-semiconductor (MIS), and p-GaN gate stacks while accounting for possible GaN buffer types (Fe-doped and C-doped). A strong correlation between 3-terminal (3T) breakdown voltage, gate design, and relative concentration of various charges was found. % increase in 3T breakdown voltage when physical dimensions were doubled was also found to be strongly correlated with the relative concentration of various charges for both Fe- and C-doped buffer HEMTs. On the other hand, the 2T (source–drain, without gate, and GaN channel below gate) breakdown voltage was independent of all other parameters except buffer properties and physical dimensions. Physical insights are developed to explain the dependence of electric field distribution, carrier injection, and HEMT breakdown on the surface states, polarization charge, and buffer traps, as well as their relative concentrations for both the buffer types and all three gate types. These insights will help to design efficient surface passivation schemes and resolve ambiguities, often observed in experiments, in terms of location of peak electric field (drain side, or gate side or both) as well as OFF-state conduction and breakdown mechanism (gate injection, or punchthrough, or parasitic conduction through buffer or avalanche generation).**

Index Terms— **AlGaN/GaN high electron mobility transistor (HEMT), breakdown mechanism, HEMT breakdown, HEMT simulation.**

I. INTRODUCTION

OVER the years, there have been multiple mechanisms proposed for the drain current breakdown in AlGaN/GaN high electron mobility transistors (HEMTs)–1) punchthrough effect due to poor isolation provided by the buffer [1]–[5];

2) current injection at the Schottky gate [1], [4], [6], [7]; 3) vertical leakage resulting from poor growth, conducting substrate or poor compensation of the buffer layers [1], [4], [8]–[10]; 4) hopping conduction at the surface [11] and 5) impact ionization at the gate edge leading to generation of electron hole pairs [1], [4]–[7], [12]–[14]. The characteristics of time dependent breakdown of HEMT buffer is also reported in the literature [15], [16].

Uren *et al.* [3] showed the punchthrough current in undoped GaN buffer is responsible for short-channel and drain induced barrier lowering (DIBL) effects. In another study, punchthrough current and vertical breakdown have been shown as breakdown mechanisms for short channel and long channel devices, respectively, in a C-doped HEMT [17]. The previous studies on the impact of surface traps on breakdown voltage only discuss the impact of trap ionization, resulting in a "virtual gate" formation [18]. It was suggested that the surface trap ionization depletes the localized channel region and hence alleviates the gate electric field leading to breakdown. Besides, surface trap-assisted carrier transport has also been proposed as a potential reason for device breakdown [11]. However, the interplay of surface traps with the polarization and buffer charges can potentially govern the field distribution and, therefore, breakdown has not been explored. Saito *et al.* [19] have shown impact ionization dominating at drain contact in undoped buffer. It has been experimentally observed that the depletion region extends from the gate toward the drain contact as a function of drain bias [20] in the case of undoped GaN buffer. Peak electric field and hence, the device breakdown occurs near the drain side of the gate edge. On the other hand, certain reports show the breakdown's physical location at the drain contact edge [12], [19], [21], [22]. This ambiguity pertaining to the electric field's spatial distribution in the device in the OFF-state breakdown condition is not addressed in the previous works.

It is worth highlighting that most of the previous investigations on breakdown phenomena studied breakdown as a function of particular design parameters, such as buffer thickness [9], surface traps [18], unintentionally doped (UID) buffer doping [3], vertical breakdown [8], [9], C-buffer doping [23], and barrier doping [24] in isolation, i.e., without considering interplay or interdependencies on other parameters. Besides, the majority of earlier works were limited to UID GaN buffers and/or Schottky-gated HEMTs. This limits our understanding.

Since the electric field is a function of charge distribution across the entire system, from the device design point of view, the interplay of various charge sources and its implications on field and breakdown voltage must be explored in detail. We have observed that the electric field profile in HEMT is a strong function of 2DEG concentration, defined by the surface and polarization charges. Besides, it is a function of buffer traps as well as gate-stack design. Dependence of field distribution and breakdown voltage on the interplay of various charge sources and gate-stack design is not intuitive or trivial to visualize like a p-n junction. Besides, findings from other works mostly limited to UID GaN buffers and/or Schottky-gated HEMTs cannot be extended to p-GaN/metal-insulator-semiconductor (MIS) gate stacks as well as Fe/C-doped GaN buffers. Keeping these gaps in mind, this manuscript adds the following to the state-of-the-art known to date: 1) the interplay of various charge sources (from the surface, buffer, and polarization) in AlGaN/GaN HEMTs governing the electric field distribution and breakdown mechanism, 2) investigations for a range of surface and buffer trap concentrations as well as polarization charge density as the prior works did not explore the same for the entire range to develop deeper insights and 3) exploration of 1) & 2) for different gate-stack design (i.e., MIS-gate, p-GaN as well as Schottky gate).

II. COMPREHENSIVE FRAMEWORK AND INTERPLAY

A. Computational Setup and Calibration

As briefed above, the prior art is limited in terms of explored design space and presents findings limited to very few technology parameters (e.g., undoped GaN buffer and Schottky-gated HEMTs). Besides, previous works did not address the ambiguities observed across various experimental works. Experimentally, it is not easy to cover the entire design and technology space to understand the interplay of various parameters. Moreover, probing physical mechanisms often becomes infeasible using experiments. On the other hand, computational modeling offers a time and cost-effective way to cover the entire design space and probe more in-depth, which can explain experimental inconsistencies and/or can be used to derive efficient design guidelines.

To meet this objective, it is essential for the computational setup, as used in this work, to be reliable, which successfully reflects the experimental trends. The simulations are performed using the Synopsys Sentaurus TCAD suite. The details of transport, breakdown, and leakage calibrations are explained with experimental validation in our earlier work [25]–[29]. To highlight the key model parameters relevant to this work, it is worth pointing out that the Impact Ionization (II) induced carrier generation was considered according to Chynoweth law with electron and hole ionization parameters adapted for GaN [25], [26]. The breakdown voltage is defined at the OFF-state drain current of 1 mA/mm. Besides, models for trap-assisted transport and Poole Frankel emission across the GaN buffer were considered. Gate leakage has also been calibrated in the setup used. Our earlier works [25]–[27] show good agreement with experiments in terms of leakage and breakdown characteristics for devices realized over a
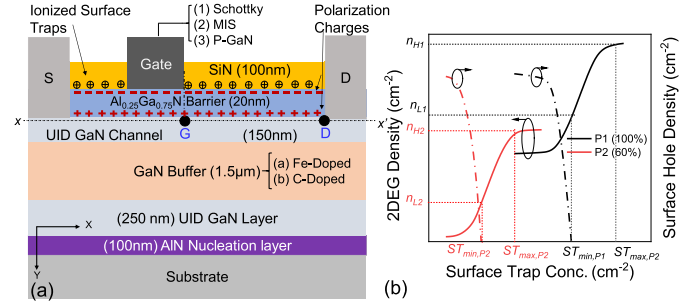

Fig. 1. (a) Cross-sectional schematic of the HEMT device used for the simulation studies. The physical device parameters are: source to gate length (L_{sg}) = 1 μm, gate length (L_g) = 0.7 μm, gate to drain distance (L_{gd}) = 5 μm or higher, channel thickness ($t_{channel}$) = 150 nm, and buffer thickness (t_{Buffer}) = 1.5 μm. The dielectric thickness in case of MIS stack was 20 nm. Whereas, pGaN stack consists of 15 nm Al$_{0.2}$Ga$_{0.8}$N barrier, 70 nm p-GaN gate layer with Mg doping of 3×10^{18} cm^{-3}. The gate terminal was biased at ($V_t - 3$) V, with source grounded, for all the 3-terminal (3T) breakdown simulations, where V_t is the threshold voltage. The substrate was undoped and kept floating to match the experimental conditions and to isolate substrate-induced breakdown effects. High acceptor trap concentration of 3×10^{18} cm^{-3} is assumed in the AlN nucleation layer and at the Substrate-AlN interface. It should be noted that the field plate was not used for investigation conducted in this work. (b) Upper and lower limits of 2DEG density, for two different polarization P_1 (100%) and P_2 (60%), as a function of surface trap concentration.

Carbon (C)-doped GaN buffer. The device schematic and the respective parameters under study are shown in Fig. 1(a) and its caption.

B. Charge Sources: Polarization, Surface, and Buffer

It is known that due to strain relaxation in the AlGaN layer, the standard polarization charge may be lower than theoretically expected, which directly affects the maximum achievable 2DEG density. To account for the experimental scenario, it is necessary to account for a possible range of polarization strength and its implications on 2DEG, which should affect the space charge distribution and the electric field profile. The piezoelectric charge is computed according to $q_{PE} = -\nabla P$, where P is the total polarization vector given by the sum of spontaneous and piezoelectric polarization. The other sources of charges in the system should further modify the electric field, as described by this equation: $\nabla \cdot (\epsilon \nabla \phi) = -(q(p - n + N_D - N_A) + q_{PE})$. Here q_{PE} is the total charge induced due to polarization, ϵ is electrical permittivity, ϕ is electrostatic potential, n and p are electron and hole densities in the system, respectively; whereas N_D and N_A are ionized donor and acceptor concentrations, respectively, in the system. These ionized donors and acceptors are contributed by the surface as well as buffer traps. Besides, they can also affect the mobile charge profile in the 2DEG. Unlike the polarization charge, surface and buffer traps are dynamic in behavior, as the ionization is a strong function of applied bias, which can dynamically alter or redistribute the space charge distribution, hence the electric field profile. This aspect was never accounted for in earlier works due to the fixed charge assumption.

For a fixed polarization charge, the 2DEG density is defined by the concentration of donor type surface traps at the AlGaN
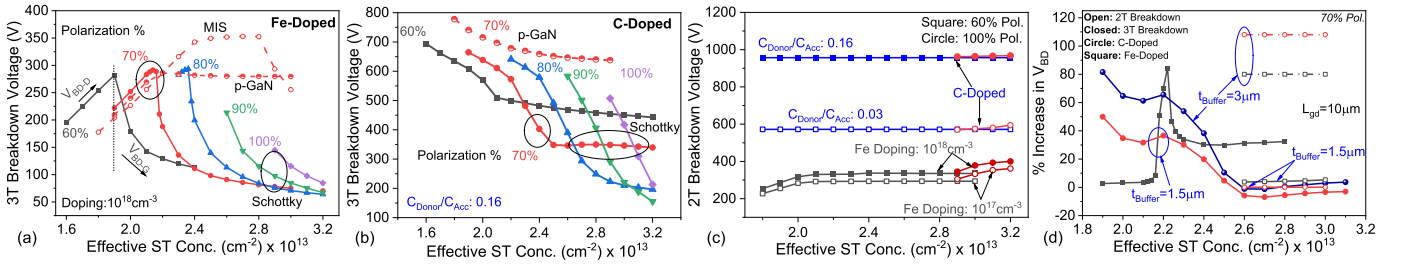
Fig. 2. 3T breakdown voltage as function of surface trap concentration for different polarization percentages and gate designs, for (a) Fe-doped and (b) C-doped buffers, while keeping L_{gd} = 5 μm and t_{Buffer} = 1.5 μm. V_{BD-D} and V_{BD-E} represent the breakdown at drain and gate edge, respectively. (c) 2T breakdown voltage for both Fe-doped and C-doped buffers depicting zero dependence on surface trap and upper limit of achievable breakdown voltage set by the buffer parameters. (d) % improvement in 3T & 2T breakdown voltage, as a function of surface trap concentration, when L_{gd} and t_{Buffer} were increased from values used in (a) and (b) to values marked inside the chart. Here the gate and region beneath the gate (from AlGaN surface to GaN channel) were removed for 2T (source–drain) breakdown simulations. The 3T breakdown corresponds to ramping drain voltage with off-state bias applied at gate. The source is kept grounded.

surface and at the AlGaN/SiN interface, introduced by the SiN passivation layer. Here, both the sources are considered, and the net trap concentration is referred to as effective surface trap concentration. In the case of polarization charge P, a minimum concentration of donor-like surface traps (ST_{min}) is required to compensate polarization-induced free hole gas at the AlGaN surface. The electrons emitted by the ionization of these donor states are swept to the channel by polarization-induced electric field, leaving the positively charged donor traps at the surface. This process continues until the polarization field in the barrier layer balances the opposing electric field between donor states and 2DEG. Subsequently, at a certain surface trap concentration (ST_{max}), the Fermi level is pinned at the surface, which stops the further transfer of donor electrons from the surface to the 2DEG. Keeping this discussion in mind, for a fixed polarization charge, we can define an upper and lower limit of sheet density that is a function of surface trap concentration, as illustrated in Fig. 1(b). Here, two sets of polarization charges, P_1 (100%) and P_2 (60%), are shown with corresponding "windows" of 2DEG densities (n_s), denoted by n_H and n_L (where, $n_H > n_L$). It should be noted that the vertical electric field in the channel, which confines the 2DEG, is a function of charge present in the GaN buffer as well as the surface. Therefore, the 2DEG concentration can in general be affected by the type of GaN buffer used, which is attributed to the difference in charged impurities, dopants, or traps present across different types of buffers. To explore the breakdown mechanism concerning various charge sources and their interplay, we have accounted for the complete range of 2DEG density (n_s), which is often experimentally observed in AlGaN/GaN HEMTs. Besides, the donor type surface traps are considered at the AlGaN/SiN interface at trap energy level of $E_C - 0.68$ eV [30].

Other than dynamic surface charges and polarization charges, ionized trap charges from the buffer are also required to be considered. In this work two types of buffers are considered. First, Iron (Fe)-doped buffer with varying acceptor trap concentration having capture cross section and trap energy level as 10^{-13} cm^{-2} and $E_c - 0.7$ eV, respectively, [31]. Second, a Carbon doped buffer, consisting of a compensating trap profile. The donor and acceptor trap concentrations were

varied while keeping fixed capture cross section for electrons (5×10^{-15} cm^{-2})/holes (10^{-15} cm^{-2}) and trap energy levels as $E_c - 0.11$ eV(donor)/$E_v + 0.9$ eV(acceptor) [25], [26].

III. INTERPLAY GOVERNING BREAKDOWN

Subsequent to the discussion on various charge sources, this section reveals its interplay and role in governing breakdown characteristics. To account for all possible scenarios, as elaborated above, both Fe and C doped buffers are investigated. Besides, the impact of different gate designs (MIS, p-GaN & Schottky) is also considered. Fig. 2(a) and (b) depicts three-terminal (3T) breakdown voltage as a function of surface trap concentration for different polarization percentages and gate designs, for Fe-doped and C-doped buffers, respectively. For each case, the surface trap concentration is varied, such that the surface holes are always compensated. Fig. 2(c) shows the 2T breakdown voltage for both Fe-doped and C-doped buffers depicting zero dependence on the surface trap and the upper limit of achievable breakdown voltage set by the buffer parameters. Moreover, breakdown voltage scaling trends as a function of surface trap concentration are studied in Fig. 2(d), which depicts % improvement in 3T & 2T breakdown voltages of HEMTs & epi-stack, respectively, as a function of surface trap concentration and buffer types, when L_{gd} and t_{Buffer} were increased from 5 μm to 10 μm and 1.5 μm to 3 μm, respectively. Figs. 3(a)–(c) and 4(a) and (b) extend these trends with surface trap concentration by varying buffer trap concentration for Fe- and C-doped buffers, respectively.

Fig. 2 reveals a strong correlation between 3T breakdown voltage gate design and the relative concentration of various charge sources. On the other hand, the 2T breakdown voltage is independent of all these parameters, except buffer properties and physical dimensions. 3T breakdown voltage scaling when physical dimensions were increased, was also found to be strongly correlated with the relative concentration of various charge sources for both Fe- and C-doped buffer HEMTs. Interestingly, in the case of Fe-doped buffer, for lower polarization charge, the breakdown voltage initially increases with surface trap concentration. The same, however, rolls-off and drops gradually beyond a
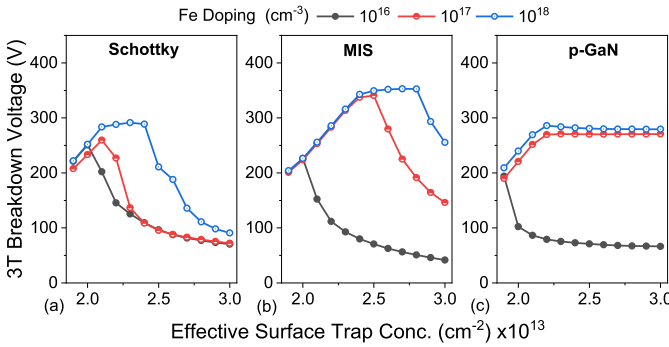
Fig. 3. Breakdown voltage codependence on surface traps and buffer doping for Fe doped buffer consisting of (a) Schottky gate; (b) MIS gate and (c) p-GaN gate stacks, respectively. 70% polarization is considered for this study.
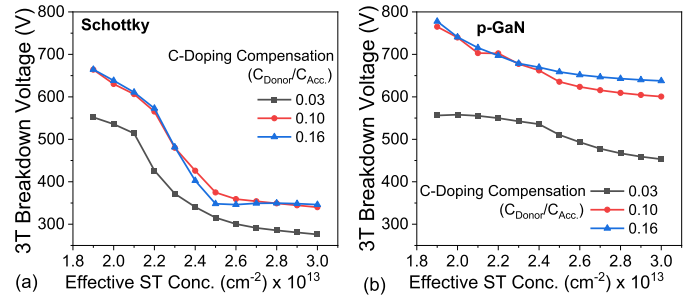

Fig. 4. Breakdown voltage codependence on surface traps and buffer doping for C doped buffer consisting of (a) Schottky gate and (b) p-GaN gate stacks, respectively. 70% polarization is considered for this study.
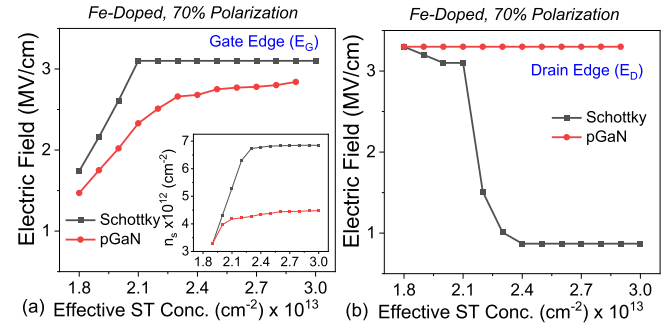

Fig. 5. Electric field strength at the breakdown in case of Fe-doped near (a) drain side of the gate edge, (b) drain edge. Inset depicts the sheet charge density as function of surface trap concentration for Schottky/MIS and pGaN gate designs.
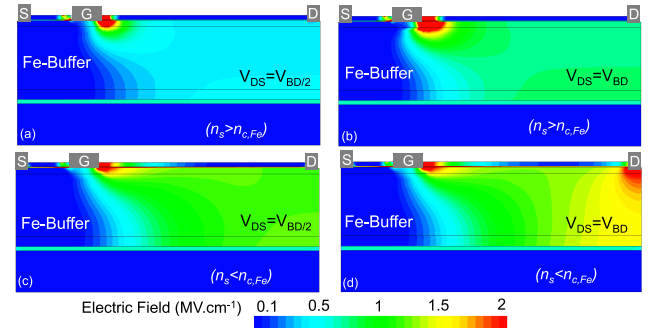

Fig. 6. Electric field contours extracted for (a), (b) $n_s > n_{c,\text{Fe}}$ and (c), (d) $n_s < n_{c,\text{Fe}}$ for different drain voltages in case of Fe doped buffer and Schottky gate design.

critical surface trap concentration. The rising part of this trend is missing for very high polarization % or sheet charge densities and, in general, for all C-doped buffer cases. In the case of Fe-doped buffer with moderate polarization % ($<$80%) and for a given gate type, while the maximum breakdown voltage appeared at different surface trap concentration values, the maximum achievable breakdown voltage was always fixed. For a moderate polarization charge, the maximum achievable breakdown voltage was found to be a function of buffer doping, as depicted in Fig. 3(a)–(c). However, the same does not hold valid for higher polarization % and in general for C-doped buffer, as the maximum achievable breakdown voltage drops with increasing polarization %. While the upper bound of the maximum achievable breakdown voltage was defined by the buffer doping and physical dimensions, as depicted by 2T breakdown voltage in Fig. 2(c) and (d); Figs. 2(d) and 3(a)–(c), 4(a) and (b) show that the relative improvement in the 3T breakdown voltage as a function of physical dimensions, or Fe/C doping is dependent on the surface trap concentration and further on the gate design. In all the cases, the breakdown voltage roll-off with surface trap concentration was slowed down in the case of MIS and p-GaN gate, which hints at the role of gate injection in governing breakdown behavior for high surface trap concentrations. Physical insights to explain these trends as well the interplay are developed in the subsequent sections.

IV. PHYSICAL INSIGHTS—IRON-DOPED BUFFER

Fig. 2(a) shows that in the case of a Schottky-gated HEMTs, for low polarization charges ($\leq$80% of maximum polarization), 3T breakdown voltage initially increases and then rolls off as a function of surface trap concentration. In this case, a distinct peak in the breakdown voltage was observed. The surface trap concentration at which the peak was observed increases with increasing polarization %. On the other hand, in the case of a higher polarization charge ($>$80%) the peak in breakdown voltage was not observed as the breakdown voltage continues to fall as a function of surface trap concentration. These trends can be explained using the electric field distribution and its evolution as a function of various parameters across the critical regions of the device. These

critical regions are the drain side of the gate edge (G) and drain contact edge (D), as shown in Fig. 1(a). In the C-doped buffer, an additional field component shown as 'bulk field' (B) is also observed, which is probed in later sections.

Fig. 5(a) and (b) show that the electric field peak shifts from drain contact edge (D) to the gate edge (G) as the surface trap concentration is increased. In general, for a fixed polarization charge, the 2DEG density in HEMT is a function of surface trap concentration, as discussed in an earlier section and shown in Fig. 1(b) as well as in the inset of Fig. 5(a). It is observed that the electric field shifts from the drain edge to the gate edge, as shown in Fig. 6(a) and (b), when 2DEG density (n_s) increases above a critical 2DEG density ($n_{c,\text{Fe}}$),

by increasing the surface trap concentration for moderate and low polarization %. Initially, in the case of lower surface trap concentration, the maximum field was positioned at the drain edge, which spreads toward the gate as the surface trap concentration was increased. This explains the rising part of the breakdown voltage vs. surface trap concentration curve. For lower polarization and lower surface trap concentrations, n_s was always less than n_c. Therefore maximum field was localized at the drain edge (D), as depicted in Fig. 6(c) and (d). This is the case with the p-GaN gate device too. The field gets localized at the gate edge for higher surface trap concentration, responsible for the roll-off behavior. This behavior is consistent for any arbitrary polarization value. For higher polarization, however, the peak field's position was always observed at the gate edge (G). In general, for higher polarization (independent of surface trap concentration), n_s is always greater than the critical value ($n_s > n_c$), therefore the electric field peaks at the gate edge (G) as depicted in Fig. 6(a) and (b). This is responsible for the monotonous fall in the breakdown voltage as a function of surface trap concentration and a drop in % improvement in breakdown voltage when device dimensions were doubled. This observed shift in electric field distribution and related breakdown dependence is explained further below.

To gain further insight into the spatial field distribution as a function of various charges, two specific cases are considered − 100% polarization and 60% polarization. Depending on the surface trap concentration and polarization, the corresponding sheet charge density for the two cases lies in the range of 10^{12} cm^{-2} to 10^{13} cm^{-2}, covering the entire spectrum of experimentally observed sheet density in HEMTs.

A. Breakdown Near Gate Edge ($n_s > n_{c,Fe}$)

While the depletion region extends from the gate edge (G) toward the drain edge as the drain bias increases, the depletion width near the gate edge is inversely proportional to the 2DEG density. Higher 2DEG density confines the space charge in a narrow region near the gate edge, which results in electric field localization. As observed in Fig. 7(a) and (b), and electric field contours in Fig. 6(a) and (b), for sheet charge density higher than critical density, gate side field (E_G) increases gradually until breakdown. The breakdown characteristics shown in Fig. 7(c) depict that the breakdown voltage is limited by the gate injection.

It is worth highlighting, as earlier observed in Fig. 2(a), that the breakdown voltage continues to decrease with surface trap concentration, even when it is increased above ST$_{max}$, i.e., where 2DEG density saturates. This suggests that the breakdown voltage not only depends on n_s but is also affected by the excess surface traps. This can be explained by analyzing the energy band diagram across the channel. Fig. 8(a) shows the energy band diagram along the device cross section at positions denoted in the inset. The localized region near the gate edge is depleted due to the Schottky junction, which leads to significant band bending in this region. This moves the
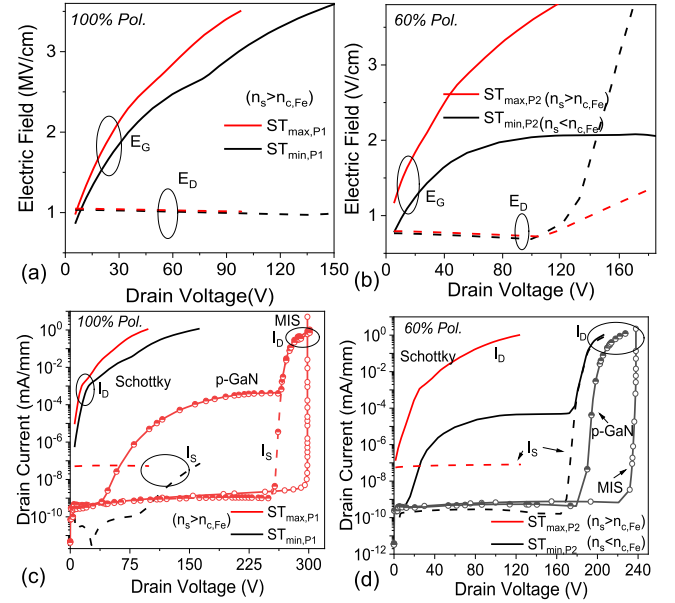

Fig. 7. Change in Electric field strength (a), (b) and total current (c), (d) as a function of drain voltage for 100% and 60% polarization in case of Fe-doped stack. For $n_s > n_{c,Fe}$, the gate field dominates, however for $n_s < n_{c,Fe}$, the electric field at drain edge increases significantly compared to gate field.
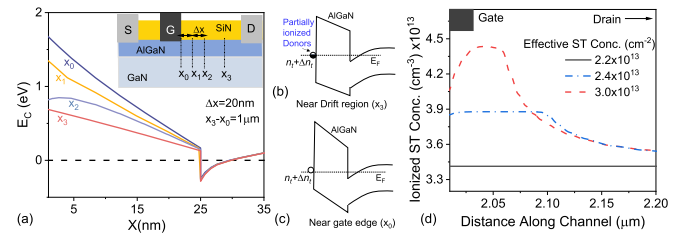

Fig. 8. (a) Conduction band energy (in the direction from AlGaN to GaN) at different positions moving from gate edge (x_0) to access region (x_3), as depicted in the schematic given in the figure inset. Here x_0, x_1, x_2 and x_3 indicate the 1D cut-positions. Energy band diagram representing the states of surface traps ionization in the (b) access region and (c) gate edge. (d) Ionized surface trap concentration near AlGaN/SiN interface along device length toward the drain.

Fermi level away from the conduction band as we move from the access region (x_0) to the gate edge (x_3). For surface trap concentrations exceeding ST$_{max}$, partially ionized traps (n_t) are present at the AlGaN surface. However, near the gate contact edge, the localized band bending leads to ionization of the excess surface states, as depicted in Fig. 8(b) and (c). This results in a higher concentration of ionized positive donor charge in the vicinity of the gate edge (G), as depicted in Fig. 8(d). The excess positive charges increase the electric field at the gate edge, enhancing the carrier injection across the Schottky gate and accelerating the breakdown process. The same is also responsible for missing breakdown voltage improvement despite increased device dimensions when surface trap concentration was increased. On the other hand, breakdown voltage improved with increasing device dimensions for lower surface trap concentration when the field was shared between drain and gate.

B. Breakdown Near Drain Edge ($n_s < n_{c,Fe}$)

For $n_s < n_{c,Fe}$, the region near the gate edge was found to be depleted at low drain bias, which results in an electric field peak at the gate edge (G), as shown in Fig. 6(c). However, the lateral extension of the depletion region is greater compared to the case with $n_s > n_{c,Fe}$. Hence the space charge here is effectively distributed across the entire drain side access region. Consequently, the peak field at the gate edge does not exceed the critical electric field with increasing drain voltage. The depletion region gradually expands and moves toward drain contact in order to support the excess drain voltage. Further, an increase in drain voltage results in space charge spreading in the vertical direction below the drain contact. Hence, the electric field at the drain edge continues to increase till impact ionization and breakdown, as shown in Figs. 7(b) and 6(d). Fig. 7(d) also shows that after the initial increase in gate leakage, the eventual breakdown occurs due to a high drain to source current. It is observed from the simulations that an alternate parasitic path is formed deep into the buffer after the breakdown at the drain, which is responsible for the high drain to source leakage in this case. It is attributed to the excess hole injection into the buffer region collected at the source via the parasitic path [32]. The breakdown voltage increases with surface trap concentration until peak value is reached, as shown in Fig. 2(a). It is attributed to an increase in the electric field peak at the gate edge (G) due to a higher n_s, which accommodates the additional drain voltage. However, the peak electric field at the gate edge remains lower than the critical field and does not initiate the impact ionization near gate contact. Increasing the surface trap concentration further proportionally increases the sheet density such that it exceeds the critical sheet charge density ($n_s > n_{c,Fe}$), resulting in impact ionization near the gate edge, which was discussed above and represented by the falling edge of the breakdown curve in Fig. 2(a).

C. Impact of Gate-stack

The breakdown voltage characteristics as a function of surface traps in the case of MIS and the p-GaN stack are also plotted along with the Schottky gate in Fig. 2(a) for comparative analysis. The corresponding electric field at the breakdown for the p-GaN stack is also shown in Fig. 5(a) and (b). In the MIS stack case, the field distribution remains the same as the Schottky gate-stack. It is worth mentioning that the position of breakdown voltage peak in Fig. 2(a) and electric field transition point in Fig. 5(a) and (b) coincide only in case of Schottky contact. In the MIS gate case, although the field shifts from drain edge to gate edge at $n_{c,Fe}$, the breakdown voltage continues to increase. This is attributed to suppressed gate injection, which delays the breakdown. Increasing the surface traps further leads to an increase in the electric field at the gate edge. This results in the generation of electron-hole pairs, which reduces the potential barrier beneath the gate, causes high drain-source leakage/punchthrough current, and eventually dominates the breakdown behavior. This explains the region where the breakdown voltage remains independent

of surface trap concentration and later falls when surface trap concentration was increased further.

The falling edge in the breakdown voltage vs. surface trap concentration characteristics was missing for the p-GaN gate HEMT. Fig. 5(a) shows that at breakdown condition, the electric field peak remains at the drain edge. It should be noted that in the case of the p-GaN stack, a relatively thinner AlGaN layer (15nm) with lower Al mole-fraction ($Al_{0.2}Ga_{0.8}N$) is utilized, which results in lower 2DEG density (5×10^{12} cm^{-2}) compared to conventional Schottky and MIS gate stacks. This is required to deplete the channel using the p-GaN gate. The maximum sheet density, in this case, is capped below the critical sheet density ($n_s < n_{c,Fe}$), resulting in an electric field peak at the drain for the entire range of surface traps as shown in Fig. 5(b). The maximum 2DEG density saturates with a further increase in surface traps, and the same is reflected in the breakdown curve shown in Fig. 2(a). While the electric field near the gate edge continues to increase as a function of surface trap concentration, the breakdown was dominated by the field at the drain. This attributed to breakdown voltage being insensitive to surface trap concentration after reaching a maximum, which is defined by the buffer doping. In case of a varying barrier thickness or higher 2DEG concentration ($n_s > n_{c,Fe}$), the electric field at the gate edge may exceed the critical value and fall in breakdown voltage, similar to MIS gate or Schottky gate will be observed. The mitigation of gate leakage by employing MIS and the p-GaN stack is shown in Fig. 7(c) and (d).

D. Interplay With Buffer Doping

While the maximum achievable breakdown voltage, i.e., 2T breakdown voltage, is defined by the buffer doping [Fig. 2(c)], the relative improvement in the 3T breakdown voltage as a function of Fe doping is dependent on surface trap concentration as depicted in Fig. 3(a)–(c). For lower surface trap concentrations, the breakdown voltage was independent of buffer doping due to early formation of drain-source parasitic conduction path (through buffer), causing drain side breakdown while having no field component present at the gate. As the surface trap concentration increases, the gate edge starts sharing the electric field along with the drain-side edge, increasing the voltage at the critical field (breakdown) condition. For this condition, increasing buffer doping delays the formation of a parasitic source–drain channel through buffer. As a result, the maximum achievable breakdown voltage increases with buffer doping.

V. PHYSICAL INSIGHTS—SELF-COMPENSATING C-DOPED BUFFER

A. Interplay of Gate-drain and Buffer Field Components

Unlike the Fe-doped buffer, the breakdown voltage was found to fall monotonously as a function of surface trap concentration. For lower polarization charge or lower sheet charge density (eg. p-GaN gate design), the breakdown voltage was less sensitive to surface traps. As depicted in Fig. 9, while the field was found to be present at the gate edge and drain edge, an additional field component deep inside
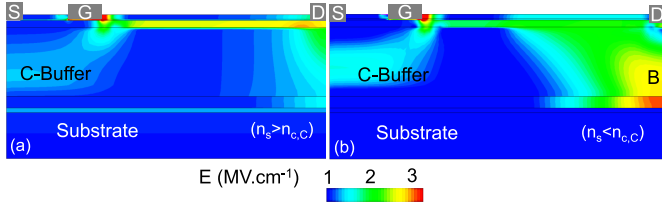
Fig. 9. Electric field contours at breakdown in case of C-doped buffer at (a) $n_s > n_{c,C}$ and (b) $n_s < n_{c,C}$.
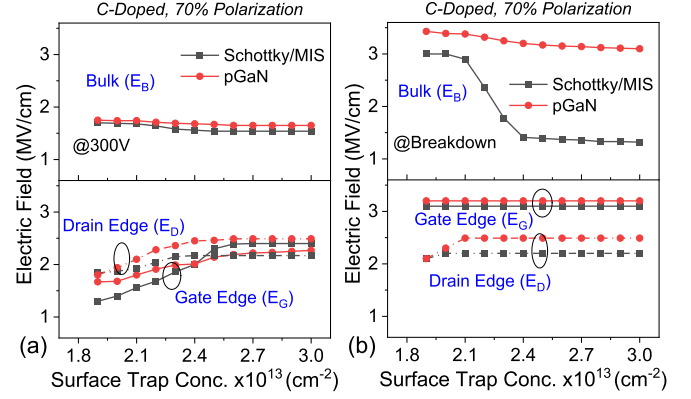

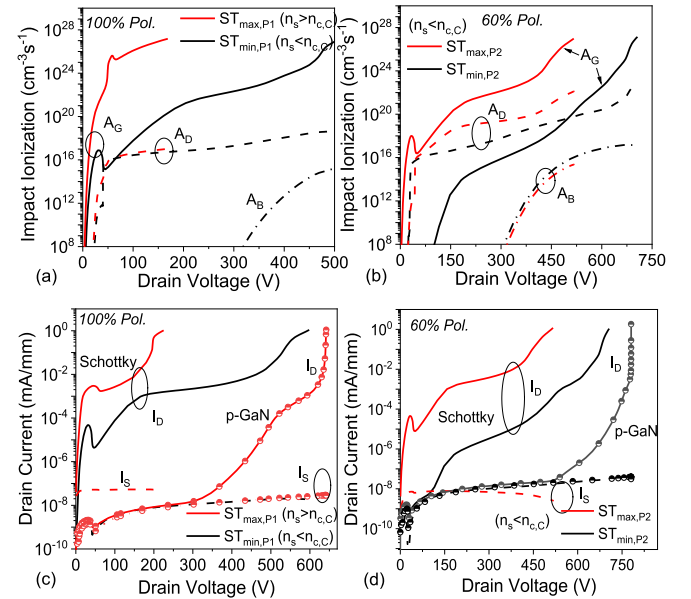Fig. 10. Electric field strength in case of C-doped buffer at (a) 300 V and (b) breakdown.

Fig. 11. Impact ionization rates (a), (b) and total current (c),(d) variation with drain voltage in case of 100% and 60% polarization for C-doped stack. A_G, A_D, A_B represent impact ionization rates at gate edge, drain edge and bulk, respectively.

GaN buffer, depicted as the bulk field (E_B), was also present in all C-doped cases. The high electric field's presence in bulk implies that the depletion region extends in both lateral and vertical directions. The self-compensating C-doped buffer consists of both ionized acceptors N_A^- as well as donor traps N_D^+. Increasing the drain bias results in the deionization of acceptor traps as the electrons trapped in the acceptor traps tend to move toward the drain. This phenomenon results in increased net positive $N_D^+ - N_A^-$ charge in the buffer. Hence the electric field gradually shifts deep into the buffer as the acceptor trap deionization increases with drain bias, resulting in bulk field component, as shown in Fig. 9(b). Due to uniform space charge distribution, the resultant electric field at the gate edge is reduced compared to the Fe-doped stack. In addition to this, the presence of bulk field component is responsible for higher breakdown voltage in the case of C-doped buffer compared with Fe-doped buffer for the same surface trap concentration and gate design.

Probing further, as shown in Fig. 9(a), revealed that for 2DEG sheet density greater than a critical density for C-doped case ($n_s > n_{c,C}$), the peak field dominated at the gate edge, followed by field strength at the drain edge and in the buffer. This is the case when polarization % and/or surface trap concentration is higher. On the other hand, for lower sheet density ($n_s < n_{c,C}$), as shown in Fig. 9(b), which is the case when both polarization % and surface trap concentration are lower, the maximum field strength was found to be inside the GaN buffer as well as gate edge. Furthermore, Fig. 10(a) shows that for a fixed drain voltage, much before breakdown (at 70% polarization), the bulk field component was fixed to a moderate value, whereas gate and drain edge field strength increases with increasing surface trap concentration. At lower surface trap concentration, all field components increase simultaneously as a function of drain voltage resulting in a high breakdown voltage attributed to the uniform distribution of field across the three regions (gate-drain and bulk). The field was still dominated at the gate edge, with the significant component present in the buffer. However, as shown in Fig. 10(b), while the gate field component dominates at the breakdown, drain and bulk field strengths readjusts to moderate and lower values, respectively, when surface trap concentration was increased. This attributes to the monotonous fall in breakdown voltage as a function of surface trap concentration.

While in the case of $n_s > n_{c,C}$, the impact ionization is relatively higher at the gate edge; the same was found to dominate at drain edge and inside GaN buffer (bulk) when $n_s < n_{c,C}$.

For $n_s > n_{c,C}$, the vertical relaxation of space charge near the drain contact is missing due to early impact ionization at the gate edge as shown in Figs. 9(a) and 11(a), (b). The bulk electric field component, in this case, is not significant. It can be observed from the OFF-state I-V characteristics, depicted in Fig. 11(c) and (d), that the drain to gate injection is the dominant conduction mechanism at the breakdown for the entire range of surface traps or sheet carrier density (n_s) in C-doped buffer. The field shared by the gate-drain, and the bulk of the device in conjunction with semiinsulating properties of C-doped buffer prevents the formation of a parasitic path, unlike Fe-doped cased, which is depicted by the low source current shown in Fig. 11(c) and (d).

B. Impact of Gate-stack and Interplay With Buffer Traps

The electric field distribution in the MIS-gate-stack follows the same behavior observed for the C-doped Schottky

gate-stack. As explained in the earlier section, the p-GaN stack consists of lower 2DEG density ($n_s < n_{s,C}$) compared to conventional stacks. Hence, a large component of the electric field is shared by the C-doped GaN buffer (bulk), as shown in Fig. 10(b). Besides, the p-GaN layer also mitigates the gate leakage component, as depicted in Fig. 11(c) and (d), which is due to reverse bias p-n-junction which requires a larger e-field for gate injection when compared with MIS-gate or Schottky gate. This results in a significant boost in the breakdown voltage for the p-GaN stack.

Furthermore, unlike Fe doping, the relative improvement in the breakdown voltage as a function of C-doping was independent of surface trap concentration, as depicted in Fig. 4(a) and (b). This is attributed to the bulk field component. For $n_s < n_{s,C}$, due to the dominance of drain and bulk fields, the breakdown voltage was less sensitive to surface trap concentration for the entire range of possible buffer doping. However, for $n_s > n_{s,C}$, when the gate field component dominated, the relative drop in breakdown voltage for different buffer doping concentrations was the same.

VI. CONCLUSION

Although the 2T breakdown voltage was independent of polarization and surface charge, we have found that spatial field distribution in HEMTs and respective 3T breakdown characteristics are strongly dependent on the interplay of surface traps, polarization charge, and buffer traps, as well as their relative concentrations. For both Fe- and C-doped buffers, unique and distinct 3T breakdown voltage versus surface/polarization charge trends were observed. For both the buffers, when $n_s > n_{c,\mathrm{Fe}/C}$, or when the Fermi level at the surface was pinned due to high donor traps, the peak field was at the gate edge leading to gate injection as a dominant 3T breakdown mechanism. This was responsible for the roll-off behavior seen in 3T breakdown voltage as a function of surface trap or/and polarization charge. On the other hand, for $n_s < n_{c,\mathrm{Fe}/C}$ it was located at the drain edge (Fe- & C-doped) as well as inside the GaN buffer (C-doped). This explains the rising part of the characteristics in the case of Fe-doped buffer and weaker dependence as well as significantly higher breakdown voltage in C-doped buffer HEMTs, at lower surface trap concentration and/or lower polarization %. Under this condition, the breakdown was due to the formation of parasitic conduction path through buffer (Fe-doped) or due to punchthrough under the gate, through GaN channel (C-doped). In the earlier case, due to the dominant gate injection, the 3T breakdown voltage did not improve proportionately when lateral spacing or buffer thickness was increased. The breakdown voltage was maximum and scalable when $n_s \sim n_{c,\mathrm{Fe}/C}$, i.e., when the field was shared between gate-drain (Fe-doped/C-doped), and buffer (C-doped) regions. For high surface trap concentration or high polarization charge, the breakdown voltage was found to be a weak function of buffer doping. The gate injection limited breakdown and roll-off in the case of the Schottky gate were mitigated by using MIS and the p-GaN gate-stack. It, however, did not improve the breakdown voltage significantly. Although these insights will help address ambiguities often observed in experiments, the comprehensive understanding developed here will help to derive unified field plate design guidelines.

REFERENCES

[1] G. Meneghesso, M. Meneghini, and E. Zanoni, "Breakdown mechanisms in AlGaN/GaN HEMTs: An overview," *Jpn. J. Appl. Phys.*, vol. 53, no. 10, Oct. 2014, Art. no. 100211, doi: 10.7567/JJAP.53.100211.

[2] M. Meneghini et al., "Electrical and electroluminescence characteristics of AlGaN/GaN high electron mobility transistors operated in sustainable breakdown conditions," *Jpn. J. Appl. Phys.*, vol. 52, no. 8S, Aug. 2013, Art. no. 08JN17, doi: 10.7567/JJAP.52.08jn17.

[3] M. J. Uren et al., "Punch-through in short-channel AlGaN/GaN HFETs," *IEEE Trans. Electron Devices*, vol. 53, no. 2, pp. 395–398, Feb. 2006, doi: 10.1109/TED.2005.862702.

[4] W. Saito, T. Suwa, T. Uchihara, T. Naka, and T. Kobayashi, "Breakdown behaviour of high-voltage GaN-HEMTs," *Microelectron. Rel.*, vol. 55, nos. 9–10, pp. 1682–1686, Aug. 2015, doi: 10.1016/j.microrel.2015.06.126.

[5] N. Zagni, F. M. Puglisi, P. Pavan, A. Chini, and G. Verzellesi, "Insights into the off-state breakdown mechanisms in power GaN HEMTs," *Microelectron. Rel.*, vols. 100–101, Sep. 2019, Art. no. 113374, doi: 10.1016/j.microrel.2019.06.066.

[6] M. Wang and K. J. Chen, "Off-state breakdown characterization in AlGaN/GaN HEMT using drain injection technique," *IEEE Trans. Electron Devices*, vol. 57, no. 7, pp. 1492–1496, Jul. 2010, doi: 10.1109/TED.2010.2048960.

[7] T. Nakao, Y. Ohno, S. Kishimoto, K. Maezawa, and T. Mizutani, "Study on off-state breakdown in AlGaN/GaN HEMTs," *Phys. Status Solidi (C)*, vol. 0, no. 7, pp. 2335–2338, Dec. 2003, doi: 10.1002/PSSC.200303405.

[8] C. Zhou, Q. Jiang, S. Huang, and K. J. Chen, "Vertical leakage/breakdown mechanisms in AlGaN/GaN-on-Si devices," *IEEE Electron Device Lett.*, vol. 33, no. 8, pp. 1132–1134, Aug. 2012, doi: 10.1109/LED.2012.2200874.

[9] I. B. Rowena, S. L. Selvaraj, and T. Egawa, "Buffer thickness contribution to suppress vertical leakage current with high breakdown field (2.3 MV/cm) for GaN on Si," *IEEE Electron Device Lett.*, vol. 32, no. 11, pp. 1534–1536, Nov. 2011, doi: 10.1109/LED.2011.2166052.

[10] M. Borga et al., "Modeling of the vertical leakage current in AlN/Si heterojunctions for GaN power applications," *IEEE Trans. Electron Devices*, vol. 67, no. 2, pp. 595–599, Feb. 2020, doi: 10.1109/TED.2020.2964060.

[11] W. S. Tan, P. A. Houston, P. J. Parbrook, D. A. Wood, G. Hill, and C. R. Whitehouse, "Gate leakage effects and breakdown voltage in metalorganic vapor phase epitaxy AlGaN/GaN heterostructure field-effect transistors," *Appl. Phys. Lett.*, vol. 80, no. 17, pp. 3207–3209, Apr. 2002, doi: 10.1063/1.1473701.

[12] Y. Ohno, T. Nakao, S. Kishimoto, K. Maezawa, and T. Mizutani, "Effects of surface passivation on breakdown of AlGaN/GaN high-electron-mobility transistors," *Appl. Phys. Lett.*, vol. 84, no. 12, pp. 2184–2186, Mar. 2004, doi: 10.1063/1.1687983.

[13] M. Wang and K. J. Chen, "Source injection induced off-state breakdown and its improvement by enhanced back barrier with fluorine ion implantation in AlGaN/GaN HEMTs," in *IEDM Tech. Dig.*, Dec. 2008, pp. 1–4, doi: 10.1109/IEDM.2008.4796637.

[14] H. Hanawa, H. Onodera, A. Nakajima, and K. Horio, "Numerical analysis of breakdown voltage enhancement in AlGaN/GaN HEMTs with a high-k passivation layer," *IEEE Trans. Electron Devices*, vol. 61, no. 3, pp. 769–775, Mar. 2014, doi: 10.1109/TED.2014.2298194.

[15] M. Meneghini et al., "OFF-state degradation of AlGaN/GaN power HEMTs: Experimental demonstration of time-dependent drain-source breakdown," *IEEE Trans. Electron Devices*, vol. 61, no. 6, pp. 1987–1992, Jun. 2014, doi: 10.1109/TED.2014.2318671.

[16] B. Shankar et al., "Time dependent shift in SOA boundary and early breakdown of epi-stack in AlGaN/ GaN HEMTs under fast cyclic transient stress," *IEEE Trans. Device Mater. Rel.*, vol. 20, no. 3, pp. 562–569, Sep. 2020, doi: 10.1109/TDMR.2020.3007128.

[17] G. Curatola, M. Huber, I. Daumiller, O. Haeberlen, and G. Verzellesi, "Off-state breakdown characteristics of AlGaN/GaN MIS-HEMTs for switching power applications," in *Proc. IEEE Int. Conf. Electron Devices Solid-State Circuits (EDSSC)*, Jun. 2015, pp. 543–546, doi: 10.1109/EDSSC.2015.7285171.

[18] N.-Q. Zhang, B. Moran, S. P. DenBaars, U. K. Mishra, X. W. Wang, and T. P. Ma, "Effects of surface traps on breakdown voltage and switching speed of GaN power switching HEMTs," in *IEDM Tech. Dig.*, Dec. 2001, pp. 5–25, doi: 10.1109/IEDM.2001.979575.

[19] W. Saito, M. Kuraguchi, Y. Takada, K. Tsuda, I. Omura, and T. Ogura, "Design optimization of high breakdown voltage AlGaN-GaN power HEMT on an insulating substrate for R_{ON}A-V_{BD} tradeoff characteristics," *IEEE Trans. Electron Devices*, vol. 52, no. 1, pp. 106–111, Jan. 2005, doi: 10.1109/TED.2004.841338.

[20] N. Tipirneni, A. Koudymov, V. Adivarahan, J. Yang, G. Simin, and M. A. Khan, "The 1.6-kV AlGaN/GaN HFETs," *IEEE Electron Device Lett.*, vol. 27, no. 9, pp. 716–718, Sep. 2006, doi: 10.1109/LED.2006.881084.

[21] B. Duan and Y. Yang, "Breakdown voltage analysis for the new RESURF AlGaN/GaN HEMTs," *Sci. China Inf. Sci.*, vol. 55, no. 2, pp. 473–479, Feb. 2012, doi: 10.1007/s11432-011-4496-0.

[22] M. J. Uren, M. Caesar, S. Karboyan, P. Moens, P. Vanmeerbeek, and M. Kuball, "Electric field reduction in C-doped AlGaN/GaN on Si high electron mobility transistors," *IEEE Electron Device Lett.*, vol. 36, no. 8, pp. 826–828, Aug. 2015, doi: 10.1109/LED.2015.2442293.

[23] D. Zhou *et al.*, "Investigation of breakdown properties in the carbon doped GaN by photoluminescence analysis," *Phys. Status Solidi (C)*, vol. 13, nos. 5–6, pp. 345–349, May 2016, doi: 10.1002/PSSC.201510176.

[24] W. Saito, M. Kuraguchi, Y. Takada, K. Tsuda, I. Omura, and T. Ogura, "High breakdown voltage undoped AlGaN–GaN power HEMT on sapphire substrate and its demonstration for DC–DC converter application," *IEEE Trans. Electron Devices*, vol. 51, no. 11, pp. 1913–1917, Nov. 2004, doi: 10.1109/TED.2004.836799.

[25] V. Joshi, S. P. Tiwari, and M. Shrivastava, "Part I: Physical insight into carbon-doping-induced delayed avalanche action in GaN buffer in AlGaN/GaN HEMTs," *IEEE Trans. Electron Devices*, vol. 66, no. 1, pp. 561–569, Jan. 2019, doi: 10.1109/TED.2018.2878770.

[26] V. Joshi, S. P. Tiwari, and M. Shrivastava, "Part II: Proposals to independently engineer donor and acceptor trap concentrations in GaN buffer for ultrahigh breakdown AlGaN/GaN HEMTs," *IEEE Trans. Electron Devices*, vol. 66, no. 1, pp. 570–577, Jan. 2019, doi: 10.1109/TED.2018.2878787.

[27] V. Joshi, A. Soni, S. P. Tiwari, and M. Shrivastava, "A comprehensive computational modeling approach for AlGaN/GaN HEMTs," *IEEE Trans. Nanotechnol.*, vol. 15, no. 6, pp. 947–955, Nov. 2016, doi: 10.1109/TNANO.2016.2615645.

[28] A. Soni, S. Shikha, and M. Shrivastava, "On the role of interface states in AlGaN/GaN Schottky recessed diodes: Physical insights, performance tradeoff, and engineering guidelines," *IEEE Trans. Electron Devices*, vol. 66, no. 6, pp. 2569–2576, Jun. 2019, doi: 10.1109/TED.2019.2912783.

[29] A. Soni and M. Shrivastava, "Computational modelling-based device design for improved mmWave performance and linearity of GaN HEMTs," *IEEE J. Electron Devices Soc.*, vol. 8, pp. 33–41, 2020, doi: 10.1109/JEDS.2019.2958915.

[30] D. Bisi *et al.*, "Deep-level characterization in GaN HEMTs—Part I: Advantages and limitations of drain current transient measurements," *IEEE Trans. Electron Devices*, vol. 60, no. 10, pp. 3166–3175, Oct. 2013, doi: 10.1109/TED.2013.2279021.

[31] M. Silvestri, M. J. Uren, and M. Kuball, "Iron-induced deep-level acceptor center in GaN/AlGaN high electron mobility transistors: Energy level and cross section," *Appl. Phys. Lett.*, vol. 102, no. 7, Feb. 2013, Art. no. 073501, doi: 10.1063/1.4793196.

[32] B. Shankar, A. Soni, H. Chandrasekar, S. Raghavan, and M. Shrivastava, "First observations on the trap-induced avalanche instability and safe operating area concerns in AlGaN/GaN HEMTs," *IEEE Trans. Electron Devices*, vol. 66, no. 8, pp. 3433–3440, Aug. 2019, doi: 10.1109/TED.2019.2919491.